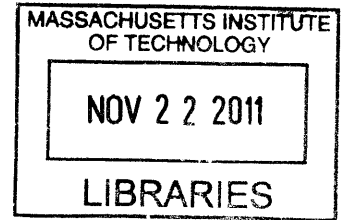Recent Lunar Magnetism

by

Jennifer Buz

S.B., Massachusetts Institute of Technology (2010)

Submitted to the Department of Earth, Atmospheric, and Planetary Sciences
in Partial Fulfillment of the Requirements for the Degree of

Master of Science

at the

MASSACHUSETTS INSTITUTE OF TECHNOLOGY

June 2011

Signature of Author ....
Department of Earth, Atmospheric, and Planetary Sciences
May 6, 2011

Certified by ....
Benjamin Weiss
Associate Professor of Planetary Sciences
Thesis Supervisor

Accepted by.................................... ....
Maria Zuber
Earth, Atmospheric, and Planetary Sciences Department Head

Recent Lunar Magnetism

by

Jennifer Buz

Submitted to the Department of Earth, Atmospheric, and Planetary Sciences
on May 6, 2011 in Partial Fulfillment of the
Requirements for the Degree of Master of Science in
Planetary Sciences

ABSTRACT

The magnetization of young lunar samples (<1.5 Ga) is a mystery because common sources of magnetic fields (e.g. core dynamo and long-lived impact plasma fields) have not been present within the last 1.5 Ga. To better characterize the source of magnetization in young lunar samples, we conducted paleomagnetic measurements on several subsamples of lunar glass 12017, which has a formation age of ~9 ka, as well as on the underlying basalt from the same sample. Various methods of magnetization were tested, including possible contamination from Earth's magnetic field, exposure to transient magnetic fields such as on the Apollo module, and interaction fields from underlying magnetized rocks. The magnetic field emanated by the rock underlying the 12017 glass was determined to be ~150 nT, comparable with the noise associated with paleomagnetic techniques. This opens up a new possible source of magnetization for samples- the laboratory. It is likely that other young lunar samples' paleointensities are overestimates, and that the strengths of magnetic fields on the Moon in the last 1.5 Ga are more similar to the strengths we observed from the 12017 glass. Underlying rocks and laboratory techniques are viable sources of magnetic fields, therefore, young lunar sample magnetization can no longer be used as evidence against an ancient core dynamo. Furthermore, the basalt portion of the 12017 is unidirectionally magnetized, suggesting an ancient core dynamo on the Moon when it formed at 3.2 Ga.

Thesis Supervisor: Benjamin Weiss
Title: Associate Professor of Planetary Sciences

Acknowledgments

Believes in aliens because he is an
Extraterrestrial himself. This is most exhibited by his
Nutty nature.

I'm infinitely grateful to my advisor Ben Weiss who took me under his wing when I was a sophomore and who, with Ian Garrick-Bethell, trained me and made me into a real-life scientist. These past few years have been incredible and I have learned and seen so much. Ben's excitement and enthusiasm for science sparked my own interests and I know that there's no going back from the path I'm on now.

Me, Ben, and Ian in the lunar sample vault at Johnson Space Center.

I owe many thanks as well to all the lab members who have helped me: Sonia, Eduardo, Laurent, Kyle, Clement, and Rachel. These guys have listened to my talks time after time, without complaining, and every time still offering valuable feedback. They also always want to debate every claim I make, which has undoubtedly made me both paranoid and more confident. Thanks, guys!

For helping me to get this far, I owe thanks to Linda Elkins-Tanton, my undergraduate advisor, and Sam Bowring, who has offered me endless advice and assistance. My committee was composed of Ben, Lindy, and Tim Grove, many thanks to them for their time and assistance.

Of course, I am also grateful to all my friends, sometimes keeping me company or bringing me snacks to lab late at night.

Lastly, I would like to thank my family for all of their encouragement and help. My parents introduced me to science through their own curiosity by taking my brother and me to aquariums, science museums, and even multiple times to the Jet Propulsion Laboratory open house. My brother has always been a role model to me through his successes.

Table of Contents

BACKGROUND LUNAR PALEOMAGNETISM

Although the Moon is our closest neighbor, we know surprisingly little about the basic interior structure of the Moon. Since the return of samples from the Moon during the Apollo program, paleomagnetic analyses on lunar rocks have been conducted in an effort to unravel some the Moon's thermal history such as whether the Moon ever had a core dynamo.

The presence or absence of an ancient core dynamo on the Moon has broad implications for the origin and evolution of the Moon. For example, a core on the Moon suggests a high degree of differentiation after accretion, which would indicate that, as the Moon was forming, it was very hot [1]. This indirectly tests the giant impact hypothesis [2] which is most consistent with a very hot (at or above solidus temperature) beginning for the Moon [3]. By comparison, the co-accretion model, in which the Earth and Moon are postulated to condense together directly out of the solar nebula, generally predicts a cool early Moon [1, 2]. Recently, with the use of lunar laser ranging and new seismic inversions of Apollo data, the presence of a small liquid outer core (r ~350 km) has been detected [4, 5].

Apollo, Luna, and Lunar Prospector data have clearly demonstrated that the Moon's crust and rocks are magnetized even though there is no active core dynamo on the Moon today [6]. One possible explanation for the paleomagnetism is that the Moon had a core dynamo in the past which has since decayed. Alternative hypotheses include impact-generated magnetic fields and magnetization by ambient magnetic fields such as from the Earth, Sun, or nearby crustal remanent magnetic fields [7].

Additionally, many samples show evidence of strong magnetic fields on the Moon present at the time of their cooling [8, 9]. A compilation of lunar paleointensity data shows that there may be a sharp increase in the magnetic field strength on the lunar surface around 4 Ga [8]. This "high field epoch" [Figure 1] [10] implies lunar paleointensities stronger than Earth's current magnetic field and has been used as evidence for an ancient core dynamo. Recently, a paleomagnetic study of lunar troctolite 76535 showed that at there was a long lived field on the Moon of at least 1 μT (and possibly 1-2 orders of magnitude stronger) at 4.2 Ga [9].

Despite this evidence for an ancient core dynamo, skeptics of the hypothesis cite the plethora of apparently young magnetized rocks (less than 1.5 Ga). Although these young magnetized rocks show magnetic fields much weaker than the proposed core dynamo, the method by which they were magnetized is unclear. Current modeling of the lifetime of a possible core dynamo on the moon predicts that an ancient core dynamo would have ceased around 2.8 Ga even assuming nontraditional, long-lived power sources [11]. Furthermore, impacts capable of generating long-lived magnetic fields are unlikely in the past 1.5 Ga [7, 12].

Without a viable understanding of the source of magnetization for the young rocks it is difficult to conclusively attribute the magnetization of the old samples to being from an ancient core dynamo.
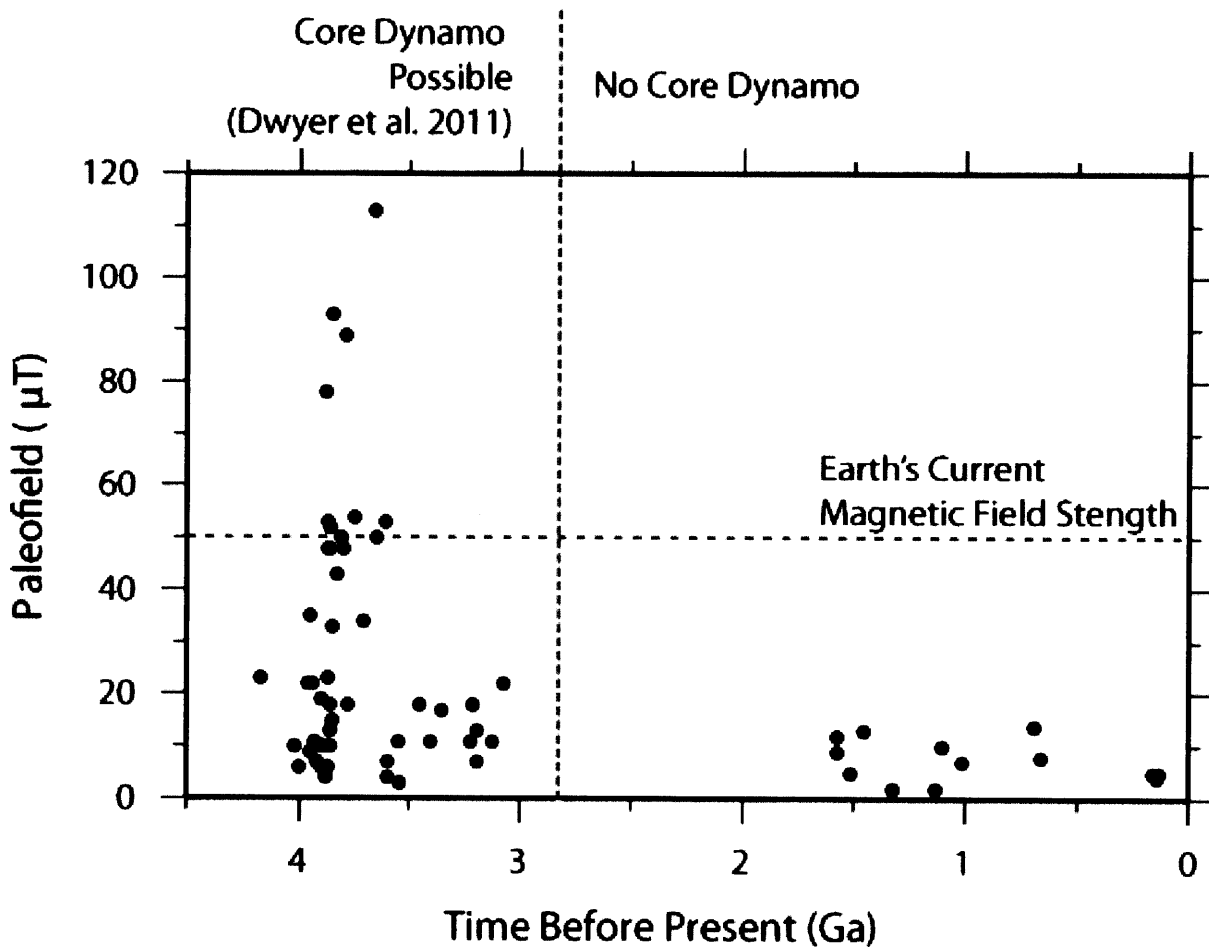

Figure 1: Lunar paleointensity variations with time

Figure modified from [10]. Note peak in field strength at ~3.9 Ga. Also note young magnetized samples at 1.5 Ga and younger. The lack of data points between 3 Ga and 1.5 Ga is a result of the rarity of returned samples in this age range. Lifetime of a nutation-powered dynamo is shown by vertical dashed line [11].

INTRODUCTION TO PALEOMAGNETISM

Paleomagnetism is the study of ancient magnetic fields recorded in rocks. Using paleomagnetism techniques, it is possible to determine the direction, intensity, stability, and duration of ancient magnetic fields. There are a variety of ways that rocks can record magnetic fields such as through cooling, residence in an ambient field for a long period of time, by short exposure to a strong field at ambient temperatures, or by shock processes. Each of these

methods for magnetization affects the rock in a unique way which can be observed through demagnetization of a sample. Although there are many methods of magnetization, I will discuss only those likely to affect lunar samples.

How Rocks Become Magnetized

Thermoremanent Magnetization

Imagine a just-solidified lava flow in Hawaii. It is likely that there are some magnetic minerals in the rock (usually magnetite and hematite for terrestrial rocks and kamacite for lunar rocks). Although there is an ambient magnetic field (the Earth's core dynamo) the thermal energy of the magnetic minerals dominates and rock behaves as a paramagnet even at temperatures well below the solidus [13]. In paramagnetic materials, unpaired electron spins act as little dipoles which can align with a magnetic field. In the case of our cooling rock, the thermal energy causes these magnetic minerals to rotate freely and the presence of the ambient field causes a small aligning torque on unpaired electron spins. Because above the Curie point the thermal energy is much greater than the aligning energy exerted by the ambient field the net moment of the rock will be small. If this ambient field is removed there will be no additional torque on the minerals and the electron spins will be randomly oriented. Paramagnetic materials are not permanent magnets.

As the rock continues to cool, it will pass through the Curie temperature, after which the material will behave as a ferromagnet. In ferromagnetic materials, adjacent moments will experience quantum mechanical exchange interactions which will collectively align them [14]. The alignment of the magnetic minerals induces a stronger net magnetization in the crystal as a whole, as compared with in the paramagnetic state when adjacent moments did not align. The alignment of adjacent moments is a result of exchange energy. As rocks cool they also condense which causes some overlap between the electron orbitals of the individual atoms. In order to satisfy the Pauli exclusion principal which states that only one electron can have a particular set of the four quantum numbers the group of nearby atoms act in concert to align themselves [14]. As each grain passes through its individual blocking temperature, it will become magnetized along its easy-axis which minimizes the anisotropy energy (which has contributions from both the shape and crystal structure of the mineral). In the case of an elongate iron grain the easy axis would be the long axis. Figure 2 demonstrates how electrons align within a mineral and give rise to a net magnetization. Getting back to our cooling rock, as each crystal passes through its blocking temperature, there is a preference for the

magnetization of the crystal to align with the easy axis closest in direction to the ambient magnetic field as this is the lowest energy configuration. The result of this alignment in the whole rock is a net magnetization direction aligned with the ambient magnetic field.

Above a crystal's blocking temperature the thermal energy required to flip the magnetization between easy axes is low and over time the magnetization will change. Below the blocking temperature the magnetization in the crystal is locked in for geologic time scales (billions of years). The result of this is an essentially permanent record of the magnetic field direction and intensity from when the rock cooled, known as thermoremanent magnetization (TRM)!

Viscous Remanent Magnetization

Because each crystal has its own blocking temperature, which may be very low, it is possible for some crystals to switch magnetization after the bulk rock has cooled. This might occur as a result of viscous remanent magnetization (VRM). Suppose that after our rock cooled to ambient temperatures, the Earth's magnetic field switched polarity. Some of the crystals in the rock with blocking temperatures near or below room temperature will be able to remagnetize. Over time the likelihood that these crystals will acquire the energy necessary to flip magnetization direction increases and slowly the rock's net magnetization changes. The net magnetization will now be the vector sum of the TRM and the VRM. The amount of VRM acquired by the sample is approximated by the log amount of time (in seconds) the sample is in the new field multiplied by the viscosity coefficient, $S = dM/d\log(t)$ for magnetization, M, and time, t [14]. Because the probability of a magnetic grain switching polarity is proportional to temperature, S increases with temperature. The energy to align with an ambient field is directly related as well to the strength of the ambient field and stronger fields will impart a VRM on samples more easily.

In most cases, VRM is viewed as a contamination of TRM. Fortunately, it is usually possible to remove VRM components through demagnetization.

Isothermal Remanent Magnetization

Isothermal remanent magnetization (IRM) is magnetization which is acquired from application of strong transient fields to materials at a constant temperature. The coercivity of a magnetic particle is related to the energy required to flip the magnetization direction. IRM will be acquired by any grain whose coercivity is lower than the IRM field [13]. On Earth lightning strikes can cause IRM because they are very energetic phenomenon associated with strong

magnetic fields. In the case of our lunar samples, it is possible that electrical systems, materials in the Apollo module, and saw blades and other equipment in the NASA lunar sample handling facility imparted an IRM [15]. Fortunately, IRM is detectable as an intense and typically non-unidirectional overprint that is easily removable through AF demagnetization.

Shock Remanent Magnetization (SRM)

Shock pressures on the orders of tens of kilobars are capable of demagnetizing or remagnetizing rock [16]. These shock pressures are easily generated by nearby meteoroid impacts. Any ambient field present at the time of the shock (e.g., dynamo field or impact-generated fields) can partly remagnetize the rock imparting an SRM. SRM is acquired by the change in pressure associated with the shock wave if a background field is present. If no field is present, demagnetization results.
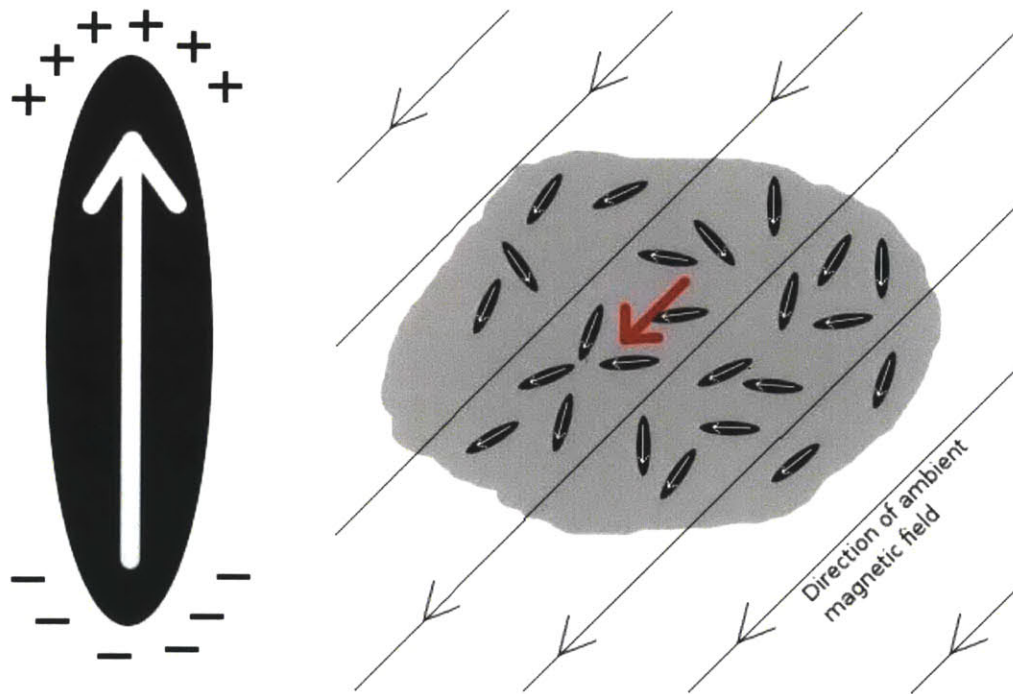

Figure 2: Magnetic crystals

(a) Representation of a ferromagnetic grain. Electrons align their magnetic moments (arrows) along the easy axis (which for iron is the axis of elongation of the grain). This produces a permanent magnetization oriented toward the top of the page

(b) A rock containing many ferromagnetic grains with randomly oriented easy axes in an ambient field. The magnetic particles chose the easy axis direction which is closest to the ambient field. The red arrow shows the net moment of the rock, which is aligned with the ambient field.

Determining Magnetization Components: Demagnetization

As previously stated, various methods of magnetization affect grains based on their coercivities. Viscous remanent magnetization affects grains based on their blocking temperature which can be related to coercivity. The gold standard of magnetization in lunar samples is uncovering any TRM. TRM is likely to be locked into grains with high coercivities. Therefore to access the TRM of a sample we must first remove any magnetic overprint which may affect grains of lower coercivities. We can do this through demagnetization. By removing the magnetization of grains gradually based on either blocking temperature or coercivity we can observe how the direction and magnitude of the sample changes.

Demagnetization is the removal of magnetization of a sample based either on the blocking temperature of the crystals (thermal demagnetization) or the coercivity of a crystal (alternating field demagnetization). Thermal demagnetization works by progressively heating a sample to higher and higher temperatures in a zero field. The result of this is that all magnetic grains with blocking temperatures below the applied temperature will be unblocked and reset randomly (because there no ambient field). Because thermal demagnetization affects grains based on their blocking temperature, as does VRM, any VRM component the sample acquired would be removed first. A problem with thermal demagnetization is that heating causes some alteration and recrystallization of the minerals and it is therefore somewhat destructive to the samples. For this reason, alternating field demagnetization is preferred for lunar samples, which are invaluable and currently irreplaceable.

Alternating Field (AF) demagnetization works by effectively randomizing the magnetization of crystals based on their coercivity. To achieve this randomization an ac field is applied in all three orthogonal directions within the magnetometer. The direction of the field in each axis switches polarity repeatedly and with each switch the magnitude of the field decreases slightly, like a damped harmonic oscillator (Figure 3). Each time the field is applied grains with coercivities lower than the applied field will remagnetize to a direction favorable with that field. As the direction is reversed and the magnitude decreases, the grains with coercivities lower than the initial applied field but higher than the decreased field will remain magnetized in agreement with the initial field. The result is the grains being evenly distributed in the two antipodal directions and no net magnetization. This assumes that there is a continuous range of coercivities in the rock. After each AF application, a moment measurement is taken and the

11

difference in direction and strength can be observed. For the next step the starting field is increased and the damping is repeated to zero field.

Noise Associated with Paleomagnetic Techniques

The minimum detection limit of our magnetometer is $\sim 10^{-12}$ Am^2, so any measurements weaker than this will not be reliable. Additionally there is noise associated with AF demagnetization. Anhysteretic remanent magnetization (ARM) is acquired in a rock when a low intensity magnetic field is applied in the presence of an alternating field, essentially giving it a dc bias in one direction. AF related noise takes the form of spurious ARM and gyroremanent magnetization (GRM) [17]. ARM noise likely is a result of an imperfect decay of the alternating field resulting in a non-zero mean field strength. ARM noise can be reduced by repeating AF steps multiple times and then averaging the results together. Because the effects of ARM noise increase with the strength of the peak field during AF demagnetization, therefore we increased the number of averaging steps as we demagnetized the samples. GRM affects rocks which have some degree of anisotropy and are subjected to static AF demagnetization in three axes. To combat the effects of GRM we applied uniaxial AF fields and then averaged together the output from the three orthogonal axes.

Paleointensity Determinations

ARM is nearly linearly proportional to the magnitude of the bias field. Stephenson 1974 showed that where the natural remanent magnetization (NRM) is a TRM, and AF demagnetization is used in removing both NRM and ARM, equation (1) applies, where h_T is bias field, H is peak value of AF, I_T and I_A are the intensities of TRM and ARM respectively, and f' is the ratio of spontaneous magnetization at room temperature and to that at the blocking temperature integrated over the blocking temperature distribution [18]. For an order of magnitude estimate, Stephenson proposed f' to be 1.34, an average of what was observed for lunar samples that he studied. This value is dependent on the size, shape, and domain state of the grains and can vary by up to an order of magnitude [19]. For the purposes of our order-of-magnitude study we assume $f' = 1.34$.

$$\left(\frac{1}{h_T}\right)\frac{\partial I_T}{\partial H} = f'\left(\frac{1}{h_A}\right)\frac{\partial I_A}{\partial H}$$
(1)

It is also possible to determine the paleointensity of a sample IRM. In a similar manner to ARM paleointensity, there is a correlation between the saturated IRM and the saturated ARM acquired in a 0.18 mT bias field [20]. Therefore, the amount of IRM acquired by a sample can

12

be related to the intensity of the applied field/ For IRM paleointensity determinations a calibration factor of 30 is used.
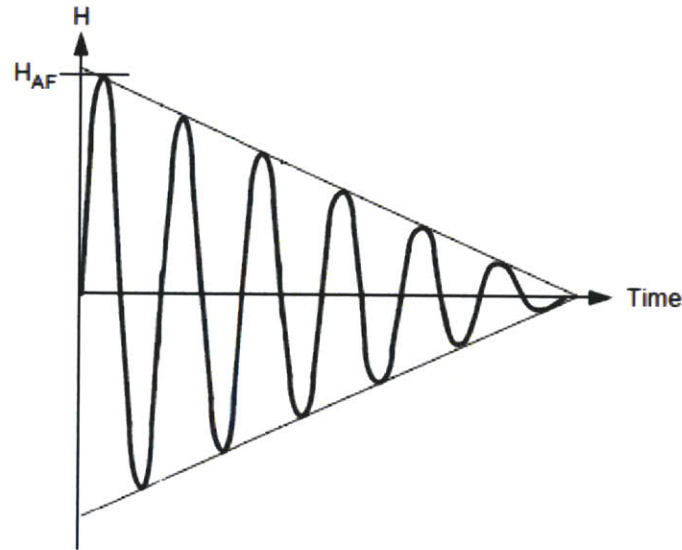

Figure 3: AF Demagnetization (Single step)

This graph demonstrates the relative direction and intensity of the applied field, H_{AF} with time. This is replicated for each of the three orthogonal axes and then a moment measurement is taken. The next AF step will have a larger initial H_{AF} . (Figure modified from Butler, 1992)
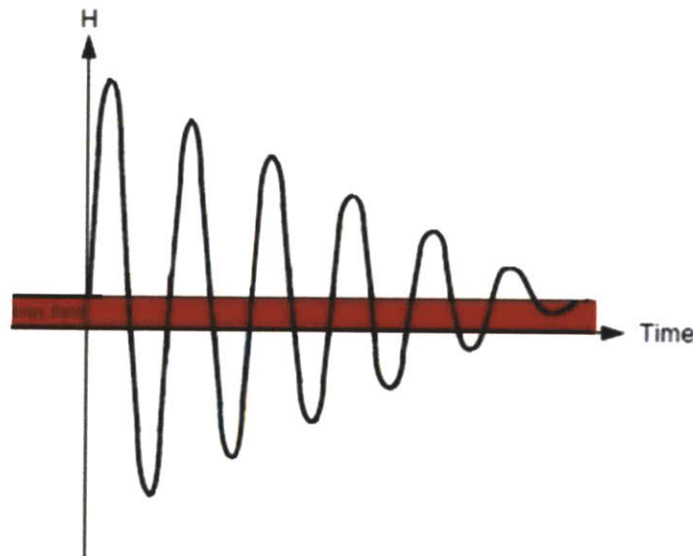

Figure 4: ARM Bias Field

The red region of this graph indicates the bias field. This bias field shifts the mean position of the alternating field in the positive direction. The rock has the ability to acquire magnetization in the direction of this bias field.

OUR EXPERIMENT AND SAMPLE

The goal of this study is to better understand and characterize young lunar samples which show magnetization and to explore possible processes by which theses samples may have acquired their magnetization. To accomplish these goals we studied a unique lunar sample, Apollo 12 sample 12017, which contains both old (3.2 Ga) material and young material (9 ka).

Sample 12017 was collected during Apollo 12, which landed in the Ocean of Storms (*Oceanus Procellerum*). The sample has not been identified in photographs from the lunar surface though its retrieval from a small mound (Figure 8)(Figure 9) during EVA1 has been assumed since it is the only sample with a glassy exterior. The small mound is speculated to have formed from an impact and it has been suggested that the glass on sample 12017 is related to its formation [21]. Alan Bean was presumably drawn to the small (52 g) sample by glints of the sun on its glass and it is therefore likely that the glass coating was facing up when found...

"118:01:47 Bean: Hey, here's a rock they'll be glad to see in Houston.

"118:01:50 Conrad: Good.

"118:01:51 Bean: It's an interesting one. It looks like a solid glass chunk. It's a real shiny black. Did you ever see anything like it before?

"118:03:39 Conrad: Put this rock in your pack. (Garbled) look at that, got that glass spatter on it. That's fantastic.

"118:03:50 Bean: Never seen anything like that rock.

"118:03:52 Conrad: No, I haven't. No, I haven't."

-Apollo 12 Transcripts, Astronauts referring to lunar sample 12017

Apollo 12 lunar sample 12017 is composed of two main lithologies: basalt and glass. The majority of the sample (>80%) is a quartz normative pigeonite basalt [22][23]. Approximately half of the exterior of the basalt has a thin (<= 5 mm) glass coating which was apparently splashed onto the basalt from a nearby impact [22] (Figure 5). Sample 12017 basalt is porphyritic with a medium grained variolitic to subophitic ground mass [23]. The plagioclase crystals are ~.19 mm wide (Fig 6) with subparallel to random orientation. 12017 is classified as a quartz-normative pigeonite basalt [23][24]. Pyroxene crystals are approximately 0.7 mm in diameter including augite rim (approximately 1mm thick). In thin section the glass is light brown with some flow banding. On the hand scale the glass appears jet black and has been described as having the luster of "polished molybdenum". The coating of glass ranges in thickness from a

few mm to <1mm. Atop the black glass is a second glass splatter in the form of a series of greenish-brown ellipses ranging in size from <1mm to 2mm [21]. This secondary glass is either from a separate, later event or from the same event but later, the young age of the glass makes the latter explanation more likely. The glass contains vesicles ranging from .1mm to a 3 mm in diameter which were observed in thin section [Figure 6]. There are some entrained crystals in the glass, primarily along the basalt-glass boundary which are presumably from the underlying basalt.

The ^{39}Ar-^{40}Ar age of the basalt is 3.19 ± 0.07 Ga [25]. We recently confirmed this age in collaboration with David Shuster at the Berkeley Geochronology Center (data not shown). Micrometeorite counts on the glass indicate an exposure age between 4-20 ka [26]. Although the exposure age only tells the time the rock sat on the surface it is likely that it is a good estimate of the age of the glass. The glass, being a splatter from a nearby impact, must have been emplaced while the rock was on the surface. If the exposure age is not a true age then the rock would had to have been both buried and resurfaced within the 20 ka exposure age range. This makes for a very complicated and improbable history. Furthermore, the exposure age is verified with the 9 ka age from spallation tracks of annealed crystals within the glass. The glass itself is only capable of preserving spallation tracks within the last 500 years [27]. An upper limit on the age of the glass is 6 Ma which is given by the catastrophic rupture of rocks on the lunar surface of a similar size [28].

No shock features (indicative of shock pressures higher than 5 GPa) such as microfracturing of plagioclase or the development of multiple twin lamellae in clinopyroxene are present in the rock [29]. Petrographic studies of the glass show that it contains unusually high abundances of most trace elements, implying addition of meteoritic material [22][30]. Using the method developed by [31] we determined the cooling rate of the basalt to be ~0.35 °C/hr and did not vary significantly with time giving total cooling time greater than two months from solidus to ambient temperatures. We calculated this using our measurements of plagioclase widths and the areal number density of pyroxene crystals (~0.8 pyx/mm^3) [Figure 7]. We approximate the conductive cooling time using a simplification of the heat conduction equation:

$$\tau \sim {l^2}/{\kappa}$$

where l is the thickness of the sample in meters and κ is the thermal diffusivity (~10^{-6}). From this we arrive at ~10 s for the thickness of our glass to cool to ambient temperatures.

Unidirectional magnetization was observed in the basalt by Strangway forty years ago [32] as well as an IRM overprint removed by ~7 mT. No paleomagnetic analysis was conducted on the glass prior to this study.

Since its delivery to Earth, 12017 has spent the majority of its time in the Johnson Space Center Lunar Receiving Laboratory. The facility is a class 1,000 clean room (there are less than 1,000 particulates of 1 μm or larger per cubic foot of space per minute). In addition, the sample was maintained in a nitrogen atmosphere to prevent oxidation. The sample was also kept under vacuum for some time. Nine months after initial characterization we further subdivided the sample using a wire saw. Detailed drawings of the subdivisions (Figure 10) have allowed us to reconstruct the relative orientation of our subsamples to one another. We were allocated several subsamples (Figure 11) that were only first exposed to Earth's atmosphere in July 2008. We subdivided samples 13A and 12A using a low speed diamond wheel saw. We separated the glass from sample 59 from the basalt using a low speed diamond wire saw in our laboratory. Water was not used in the sawing of the samples to further prevent oxidation of the rock. The difference in competency between the glass and the basalt (the glass being more competent) has allowed for natural separation of the two lithologies (see separation of 12A from 12B and 13A from 13B in (Figure 11) which occurred during subsampling at NASA. This has enabled us to conduct experiments on the two lithologies separately.
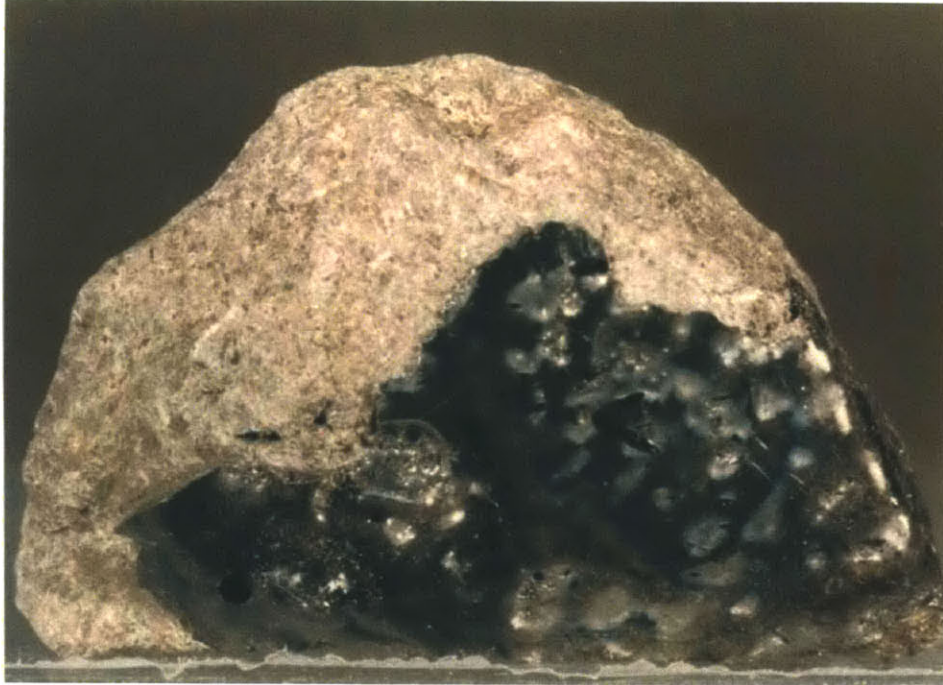
Figure 5: 12017 hand sample

Whole rock 12017. Total mass is 52 g. Underlying basalt is light gray and dull and glass splatter is shiny black. Photograph is 4 cm across. NASA photo S70-44098.
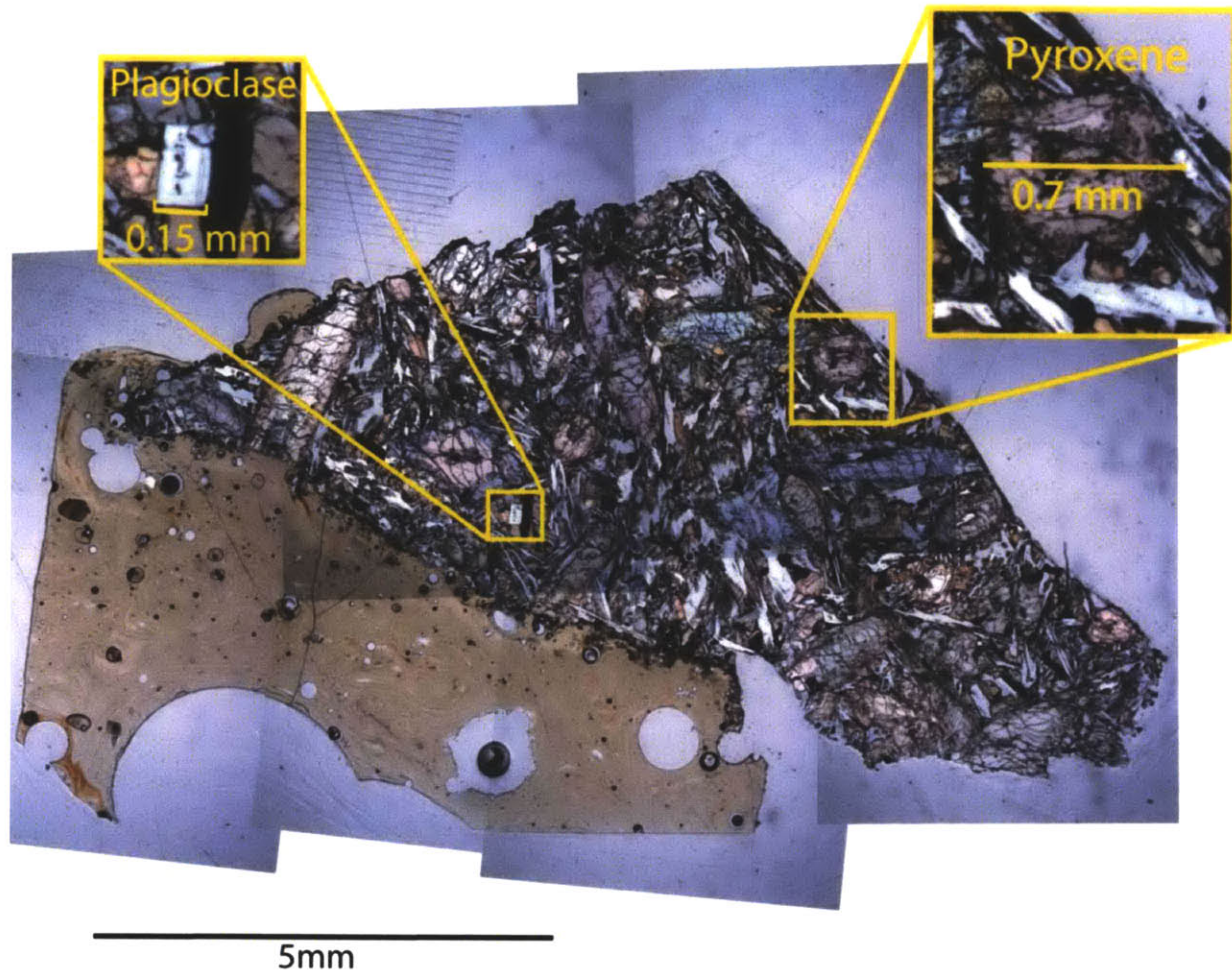
Figure 6: 12017 thin section

30 μm thin section of sample 12017 (NASA thin section # 12017,63). The brown material in the lower left of the image is the glass. Along the glass-basalt boundary there are some entrained crystals from the basalt. These entrained crystals were used to determine the age of the glass through spallation tracks [27]. We measured the pyroxene density and plagioclase widths to determine the cooling rate of the basalt. Note the augite rims surrounding the pigeonite which is distinctive of the pigeonite basalt suite of lunar samples.
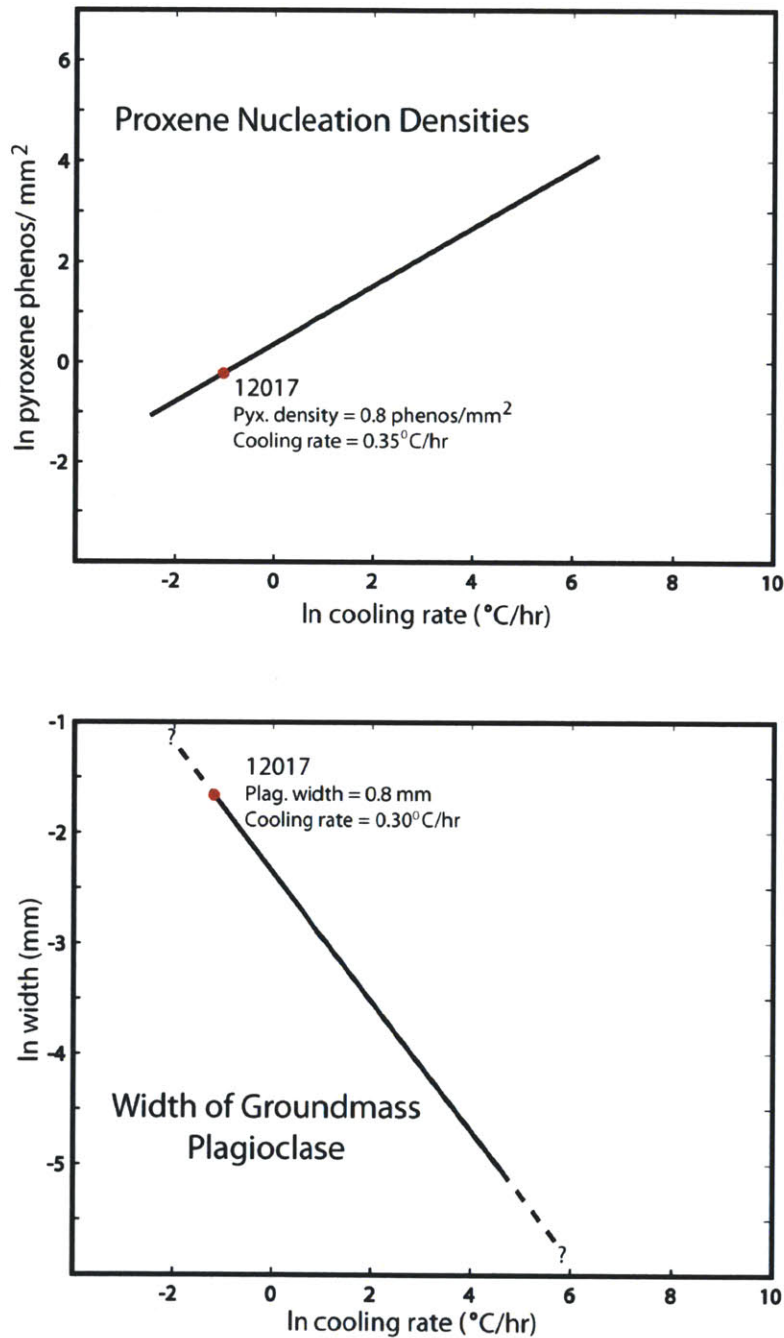
Figure 7: Cooling Rate Calculations

Experimentally determined cooling rates of Apollo quartz-normative basalts compared with pyroxene nucleation densities (0.8 pyx/mm^2) and width of groundmass plagioclase(190 μm). We determined corresponding cooling rates for 12017 with measurements on thin section 12017, 63 (Fig 4). From these, we estimate a consistent cooling rate of 0.35∘C/hr for both methods. Figure modified from [31].
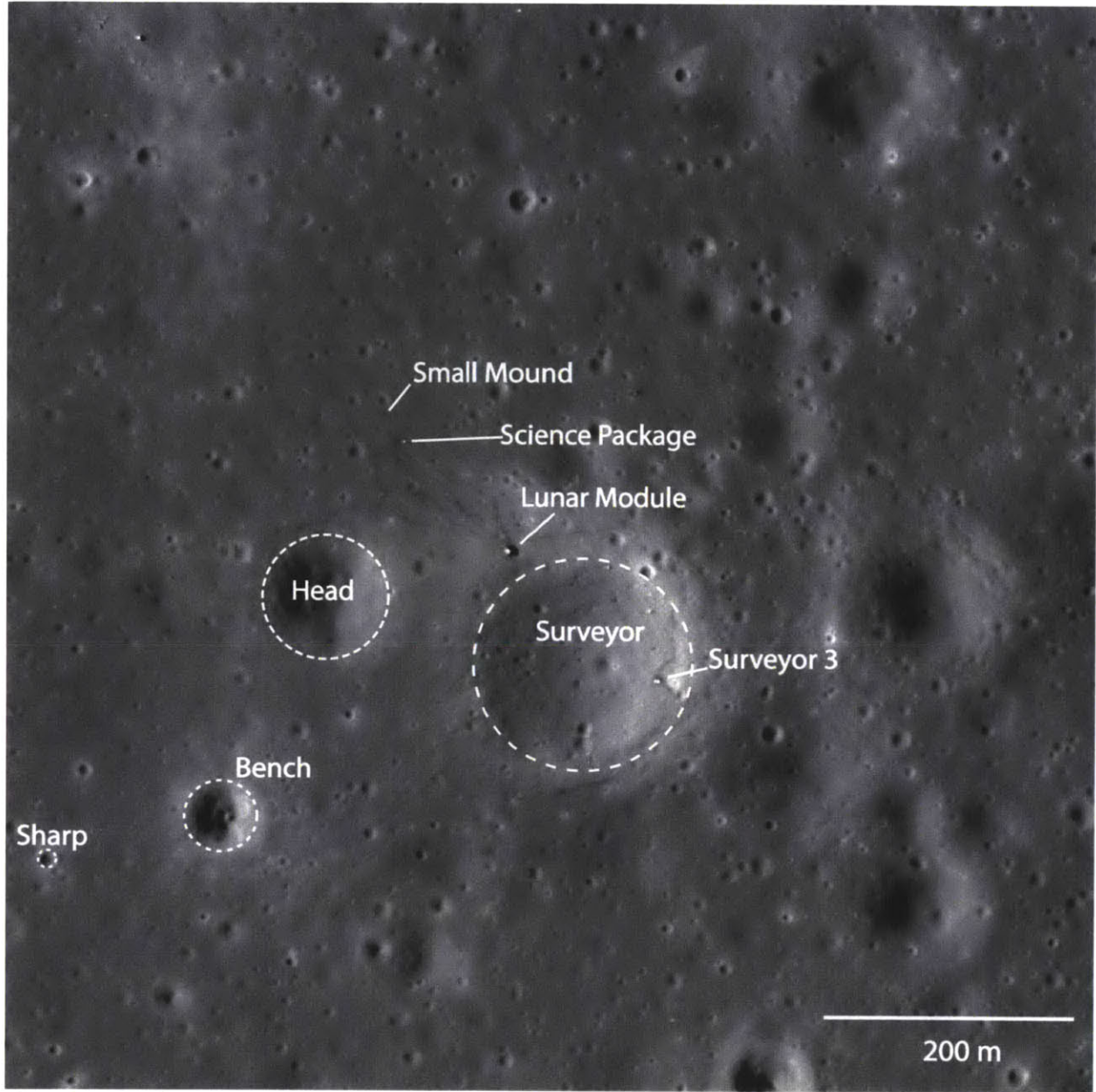
Figure 8: Apollo 12 traverse

Lunar Reconnaissance Orbiter Wide Angle Camera (LROC-WAC) photograph of the Apollo 12 landing site. Identifiable features have been labeled as well as the small mound where sample 12017 was collected. The traverse of the astronauts can be seen going between these features.
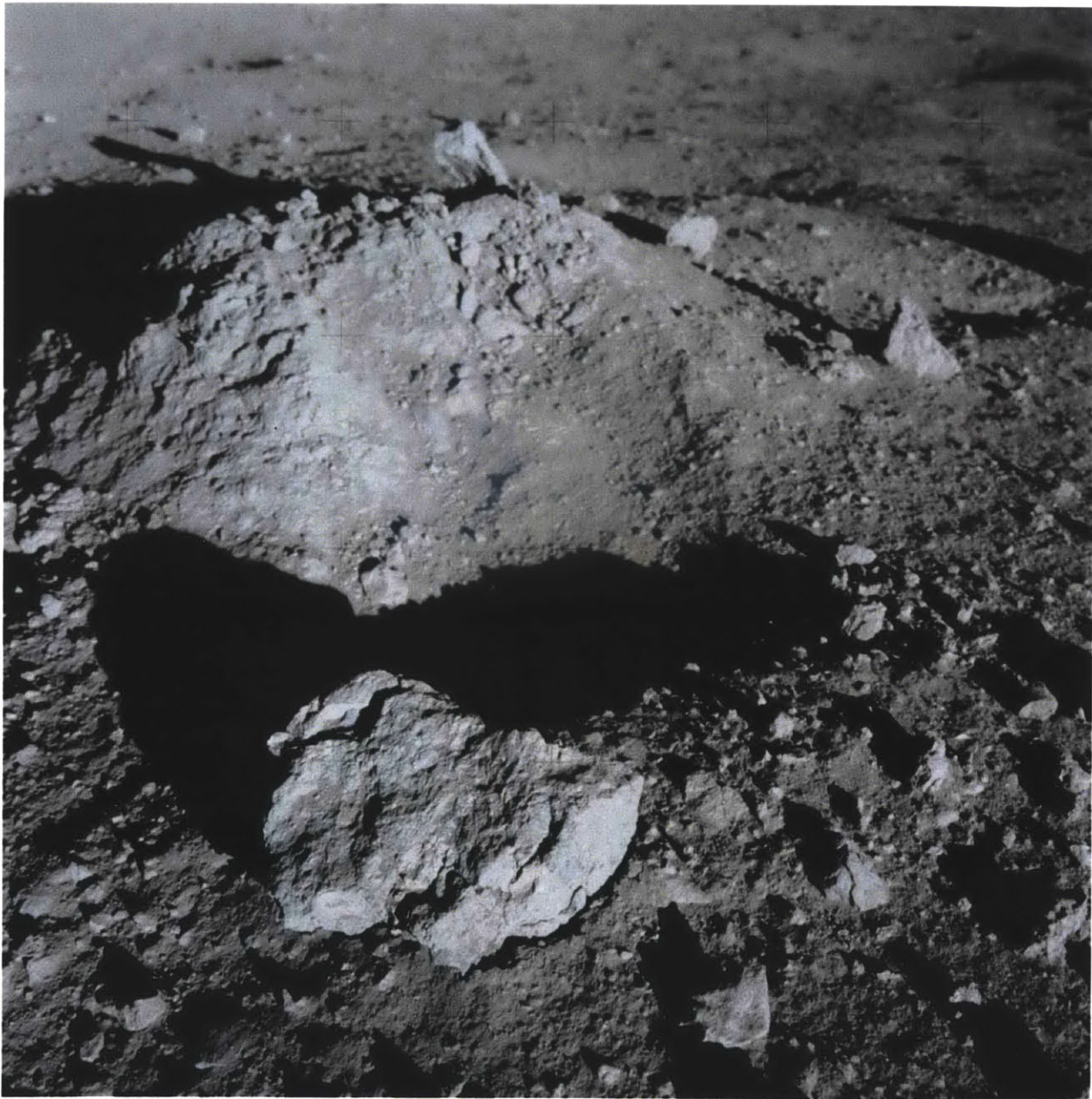
Figure 9: Apollo 12 Small Mound

Small mound where sample 12017 was retrieved (the sample is not identifiable in the photograph). NASA photo AS12-46-6825HR
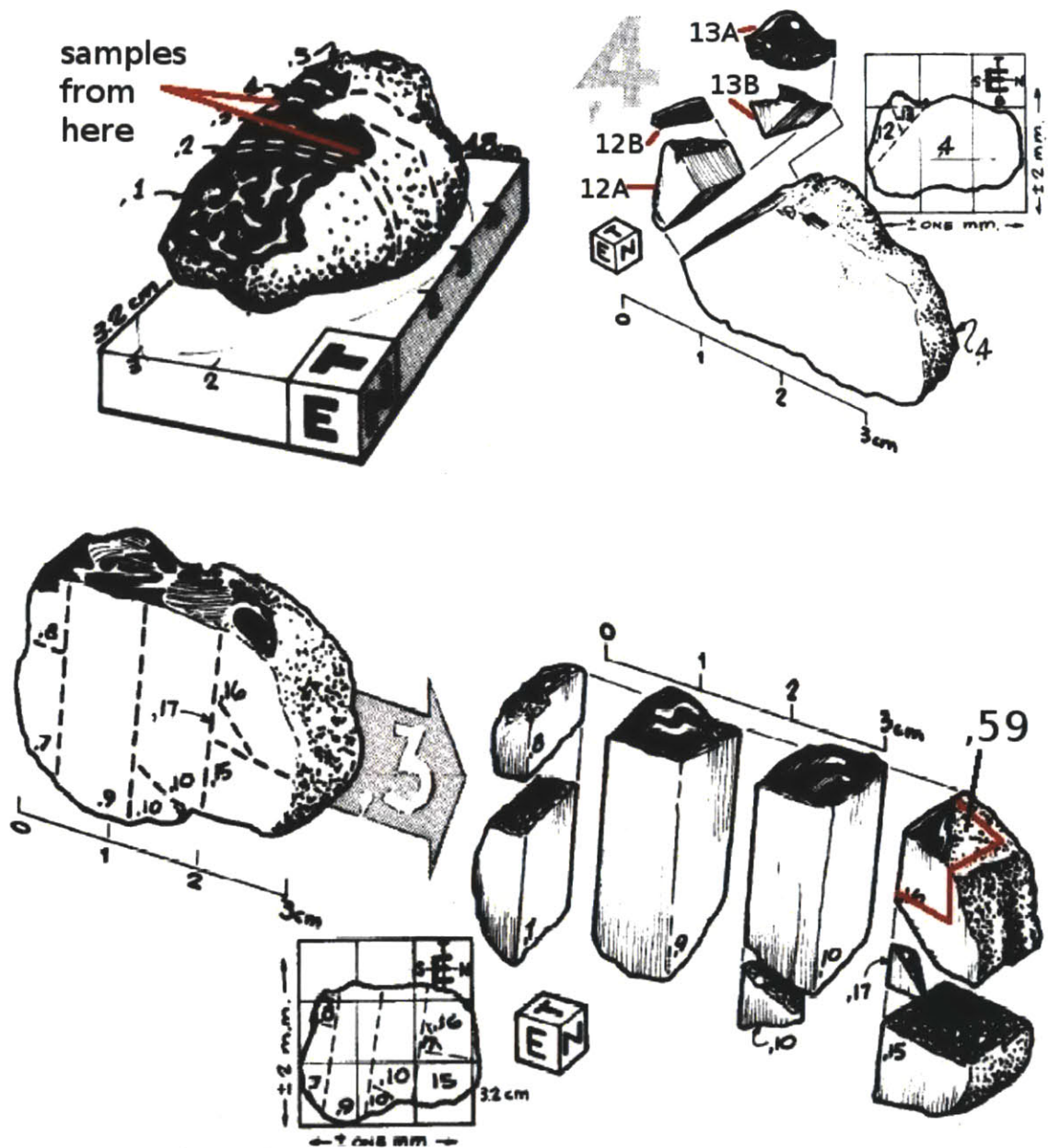
Figure 10: 12017 subsampling diagram

Illustration of saw cuts made at Johnson Space Center. The sawcuts and drawings were made in 1970. We used these drawings to reconstruct how our allocated subsamples were mutually oriented.

Figure 11a: 12017 allocation

Our 12017 allocation. Black lines indicate saw cuts made in our lab. Breaks between samples date to August, 1970 with the exception of the break between sample 12A2 and 12A1A/12A1B which occurred in our lab.

METHODS

Sample Processing

To reduce magnetic contamination, we conducted all sample processing in a class 10,000 clean, magnetically shielded room (ambient magnetic field strength ~200 nT) in the MIT Paleomagnetism Laboratory (web.mit.edu/paleomag). Also housed in this shielded room is our instrument, a 2G Enterprises Superconducting Rock Magnetometer. Because samples were cut using a metal saw at Johnson Space Center there is some risk of contamination by the saw. To reduce the effects of any possible contamination we sanded the samples using silica carbide paper until striations from the saw were removed. We observed substantial decrease in the magnetic moment as we measured the samples moments intermittently during sanding. We then reconstructed how the samples would have been oriented relative to each other in the whole rock and fixed the samples in this position to non magnetic quartz rods. We marked the quartz in order to maintain a common orientation amongst the subsamples.

Initial Measurements

The NRM of a sample is a measure of the net magnetic moment. Before demagnetization this moment is the sum of all magnetic components the rock may have

acquired (TRM, VRM, IRM, etc.). Because each subsample is capable of acquiring different magnetization after subsampling, we do not expect the direction of the NRM of the various samples to match.

Demagnetization

We started demagnetization with fields of 1.5 mT. We repeated each step four times for noise reduction and averaging purposes. We then increased the peak field by 0.5 mT until 25 mT. After 25 mT, we increased the step size to 1 mT and the steps were repeated five times. We continued demagnetization in three axes until 85 mT after which our magnetometer can only produce stronger fields in the z-axis. To compensate for this we manually rotated the samples in the three directions and demagnetized at 90, 100, 110, 120, 140, 160, 180, 200, 230, 260, and 190 mT.

Paleointensity Estimates

We applied bias fields of 0.2, 0.6, and 0.05 mT during an AF sequence similar to our demagnetization sequence in order to acquire a range of ARM acquisition curves. In an attempt to measure the capability of the samples to accurately record an ambient field present when cooling we conducted fake paleointensity experiments as well.

Paleointensity Reliability Test

We gave the samples an ARM in alternating field (Figure 4) and we then demagnetized the samples to simulate demagnetization of NRM. Using $f' = 1.34$ following [18] we then calculated the intensity of the field returned by the sample and compared this value to the strength of the applied field. We conducted this experiment at dc bias fields of 0.003, 0.02, 0.05, and 0.1 mT. The point at which the recorded field differed significantly from the applied field was considered the minimum field recordable by the sample.

RESULTS AND DISCUSSION

Magnetization Components

Moment measurements taken during sanding show that contamination from the wire saw is likely. The removal of the saw cut faces resulted in non-unidirectional sanding components and dramatic changes in the overall moment of the samples. The final NRM directions of the subsamples post sanding yielded no clear trends or obvious differences between the basalt and

glass samples Figure 12. We further subsampled some samples in our clean laboratory NRM measurements were taken prior to sawing and then again of each sample post-sawing. We added the magnetization vectors of the samples post sawing to observe if there was contamination. In the case of sawing 12A1C and 12A1B apart there was some contamination and the resultant vector was nearly 80° from the whole rock. However, for the sawing apart of 13A1 and 13A2, the resultant vector was only 10° from the pre-subsampling measurement.

After we completed sanding, we commenced AF demangetization. From NRM measurement to 8.5-10 mT, all samples (basalt and glass) exhibited a decrease in moment and clear and consistent directional changes. Zijderveld plots of this low coercivity (LC) component () clearly demonstrate that it is not trending to the origin, meaning that another, higher coercivity (HC) component is present. Plotting of least-squares fits of the LC components showed that the components are roughly unidirectional across our subsamples (), which indicates that this LC component was acquired by the whole sample after emplacement of the glass at 9 ka. Likely sources for the LC magnetization include IRM from the Apollo module or from sample handling on the Moon or at Johnson Space Center. This overprint was also identified by Strangway et al. who removed it by AF 5 mT [32]. Importantly, because many of our 12017 subsamples were sawn off the main mass just after arrival on Earth, the agreement of the LC components cannot be the result of VRM over the last 40 years. This is because, after subsampling, the individual pieces were randomly oriented for the majority of their time in Earth's field, which would prevent the acquisition of a unidirectional VRM across the samples. The samples were placed in the Earth's magnetic field for 2 weeks. When they were removed from the Earth's field we immediately measured the samples to observe the VRM acquired. We then took continuous measurements over a 2 week period to observe the decay in the VRM. From these VRM experiments, we observe that it is not possible for magnetization from Earth's field to account for more than 0.5% of the NRM. Demagnetization above ~ 64 mT revealed HC components in both basalt and glass samples. Despite increasingly noisy data (see Noise Associated with Paleomagnetic Techniques), the components were identifiable (). Some demagnetization peculiarities existed in samples 59 and 13B1, explained below.

Demagnetization of 59 revealed two low coercivity components, which we label LC1 and LC2. LC1, which was removed by 4.5 mT, does not plot near the other LC components. LC2, which is removed by 9 mT, is directionally similar to the other LC components. This suggests that LC1 was imparted to 59 after LC2 and that the magnetizing field from LC1 is weaker than that from LC2. During demagnetization of sample 59, the moment made a dramatic jump in a single step (41 mT), to ~90° from its previous direction. It then stayed at this direction until 53

mT, when it returned to its original direction. This peculiar behavior can be the result of "pinning", which is observed in highly anisotropic samples. We have yet to conduct anisotropy tests on 59, so we do not fully understand the cause of this directional jump.

For sample 13B1, we observe three clear components. 13B1 exhibits a LC component with similar coercivity range to the other samples. It then has a medium coercivity component in the south-east quadrant of the upper hemisphere, which is removed by 54 mT. During removal of the MC component, the direction makes a great circle walk to the south-east quadrant of the lower hemisphere. It seems likely that this MC component is a partial remagnetization due to heating from the emplacement of the glass. If this scenario is true, a magnetic field must have been present at the time of the glass emplacement, in order for both glass and partially demagnetized basalt to acquire a magnetization.

As previously, stated there is a general agreement of the LC components (κ=4.22) amongst subsamples, suggestive of contamination after emplacement of the glass (). Importantly, HC components of the basalt are well clustered, indicative of a unidirectional primary magnetization, likely dating back to 3.2 Ga (). Fisher statistics, which quantify the uncertainty in a mean direction, are shown in Table 2. The >2 month cooling timescale for the rock far exceeds the expected lifetimes of impact-generated fields from even basin-forming events (<1 day). The simplest explanation for the field that magnetized the basalt is a core dynamo. Given the non-ideal recording abilities of the basalt, analyses of other samples from the same period need to be conducted to more strongly promote this idea.

Because it is clear from the removal of the LC component in the glasses that some magnetization remains past the LC component, the magnetization of the glass must be resolved. The young age of the glass makes magnetization by core dynamo or impact-generated plasmas unlikely. Initially, the magnetization directions of the glass clustered significantly and it was hypothesized that the glass could have been magnetized from the underlying basalt. To test this hypothesis a map of the magnetic field of the underlying basalt was generated.

Following the procedure described in Barnett [33], we created a MATLAB program that calculates the magnetic field at all points outside our rock. From the formula for the magnetic potential due to a dipole, it is possible to solve for the magnetic potential over a volume by integrating over the volume. If the volume is uniformly magnetized, the integral can be reduced to a surface integral. This surface integral can then be transformed into a summation of integrals over the facets representing the surface. Fortunately, the basalt is apparently uniformly magnetized. Therefore, to calculate the field, we needed to first represent the surface

of the rock as a series of triangular facets. Using a cast of the hand sample made at Johnson Space Center prior to subsampling, we made our own model of this cast and then sliced it into 16 slices, each a few mm thick. We then found representative coordinates along these slices and created a digital mesh by linking the coordinates from one slice to the coordinates in another in a series of triangles. Using the paleointensity of the basalt as an approximation, we applied an ARM field of equal strength to the basalt to replicate the strength of the magnetic field at the time of glass emplacement (this assumes that the magnetization generated by the rock at the time of the glass emplacement was a result of TRM had had not been significantly demagnetized from sitting on the lunar surface). With the shape and magnetization of the basalt as inputs, we were able to predict the direction and strength of the magnetic field generated by the basalt at the location of our various glass samples. To quantify the error in the direction predictions, we also used the maximum angular deviation of the direction of the HC basalt component and observed variations.

The field of the rock was calculated along a transect passing through locations of the various glass samples studied. Although some of the measured glass directions are in agreement with the model predictions, the large scatter in the measured glass directions overall is uncharacteristic of the field generated by the basalt (**Figure 13**). Furthermore, the strength of the magnetic field in the location of the glasses is ~140 nT, comparable with the magnetic field in our shielded room. This field strength is weaker than the paleointensities of other young samples. It may still be possible that the magnetic field generated by the basalt magnetized the glass but this would not be easily recoverable using our AF methods. As we demagnetize the samples, we are imparting a spurious ARM in a bias field in the field of the shielded room, which is of the same intensity as the paleointensity recovered. The ratio of TRM produced by cooling in a given background field to ARM produced in a bias field of the same intensity is typically 0.8-20 for weak fields [18]. This indicates that the expected spurious ARM should be of equal intensity to the predicted NRM. The question then remains: why are the directions of the glass magnetizations so random as a group, even in core coordinates? Further investigation needs to be conducted but it is possible that the bias field present in the vicinity of the AF coils is changing with each measurement or experiment.
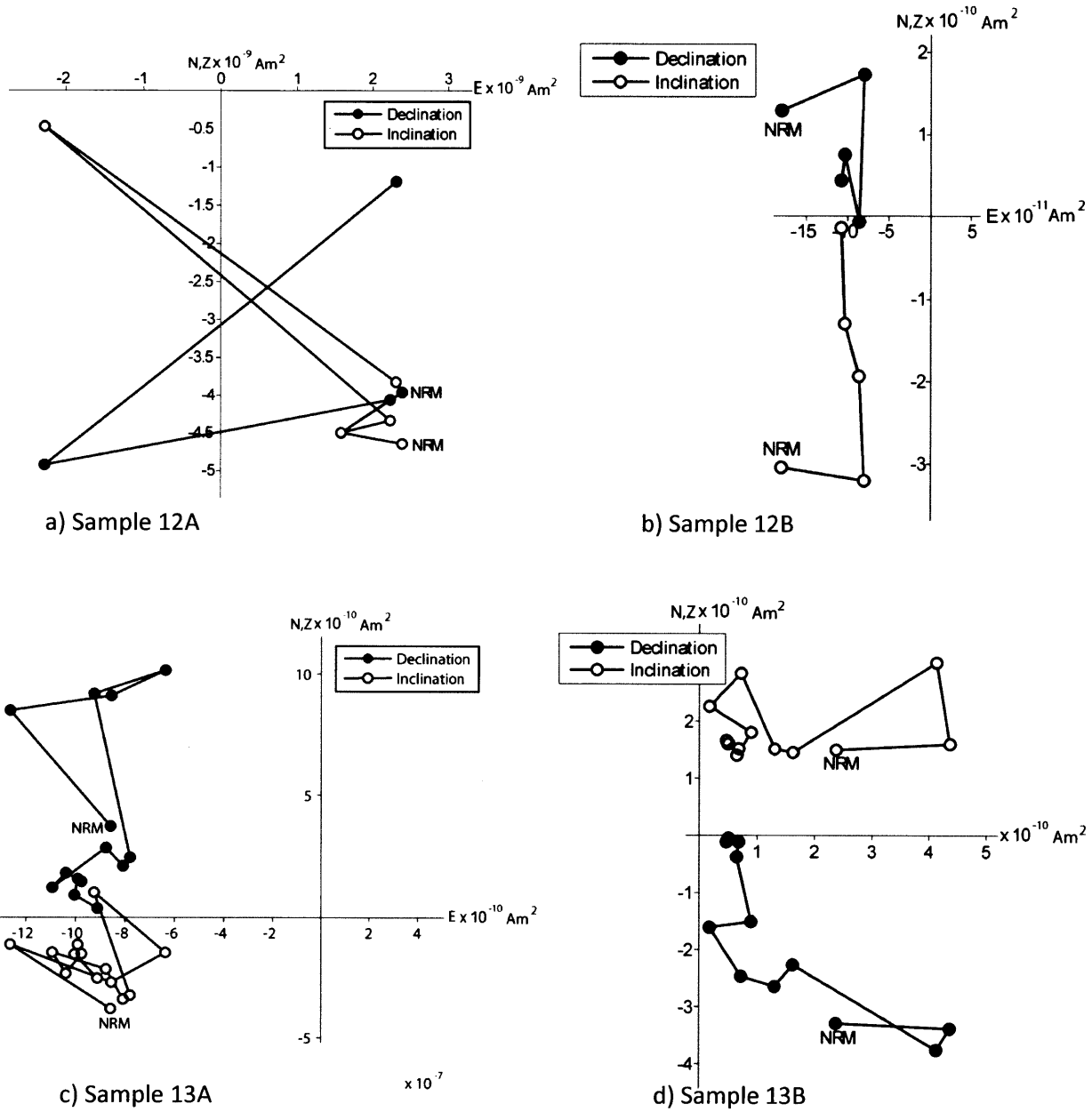
a) Sample 12A

b) Sample 12B

c) Sample 13A

d) Sample 13B

Figure 12a: Zijderveld Plots showing saw cut face removal

From these Zijderveld plots, it is clear that the magnetization imparted on the samples is non-unidirectional. Zijderveld plots are two dimensional representations of three dimensions with the vertical axis doubling as both Up and North. Closed and open symbols represent points projected onto horizontal N-S-E-W and vertical U-D-E-W planes, respectively.
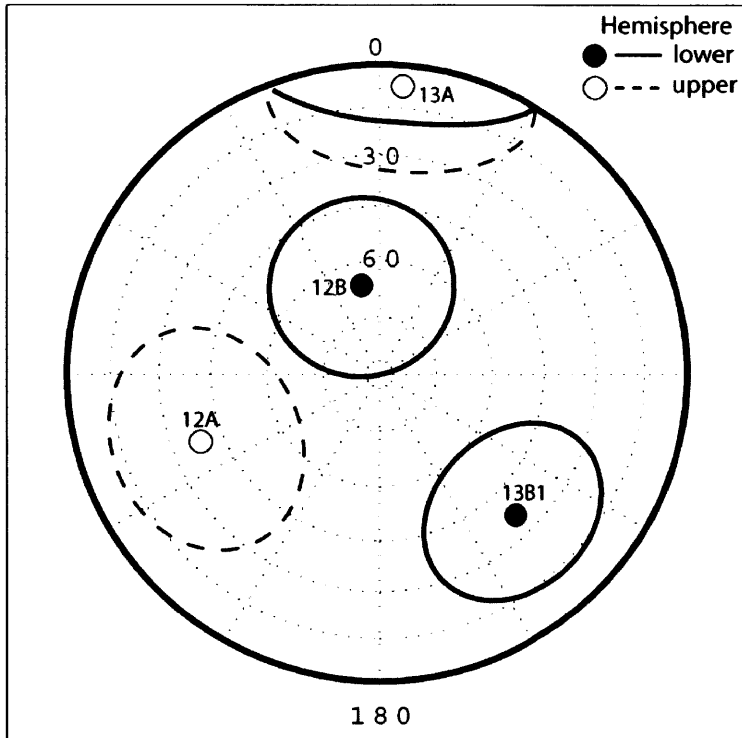
Figure 12b: Equal area plot showing saw cut magnetization components

This figure summarizes the different least squares directions from sanding. It is clear from the scatter of the various least squares fits that the sawing of the samples did not impart a unidirectional magnetization. Maximum angular deviation is also shown.
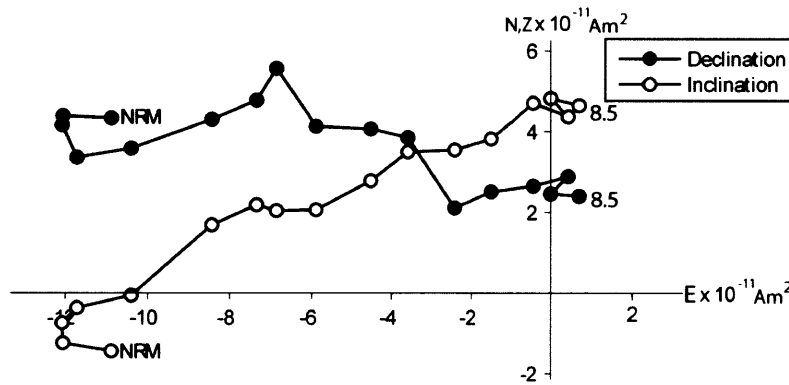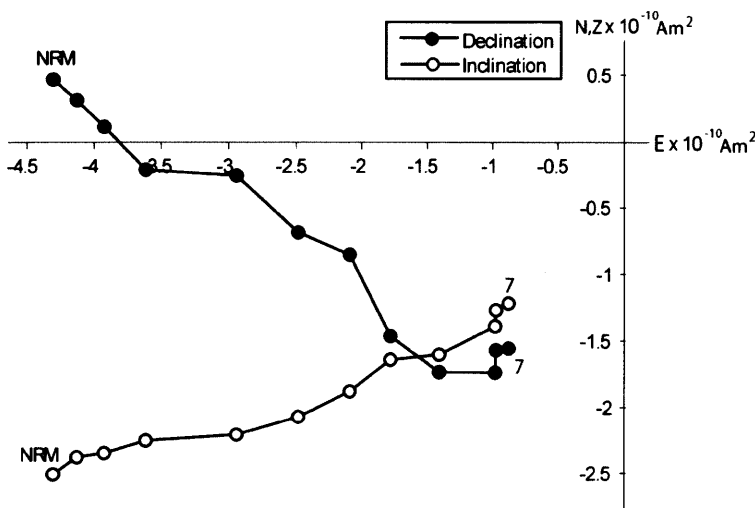

Figure 13: Demagnetization of LC component

Zijderveld Plots showing the removal of the LC component. Note how the decay is not origin-trending, as it would be if this were the only component. Also, note how similar the decay of the component is between these two samples.
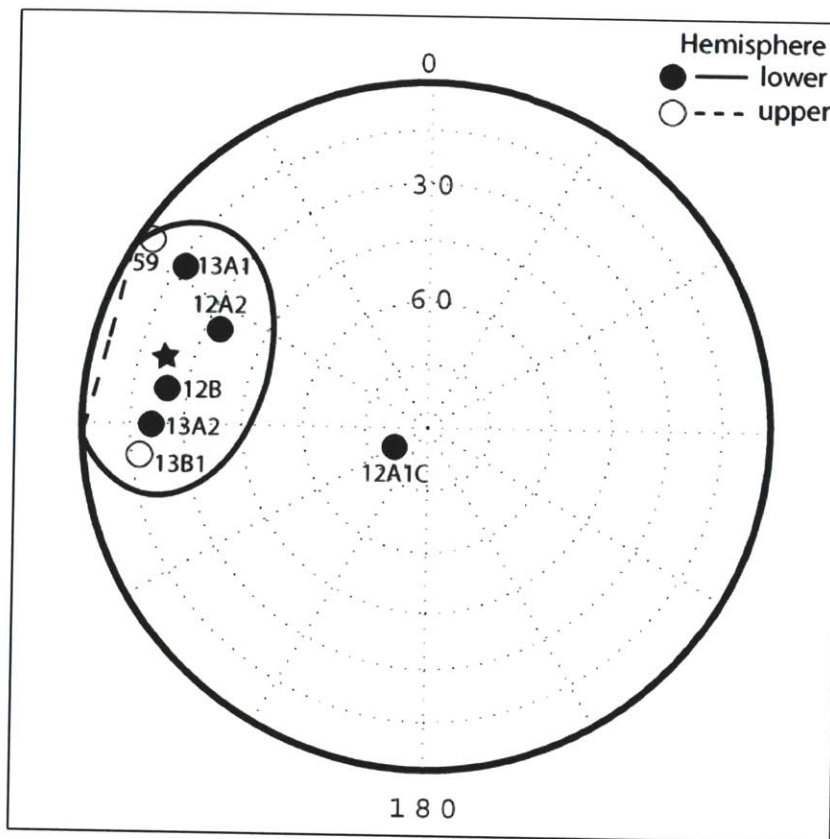

29

Figure 14: LC Components

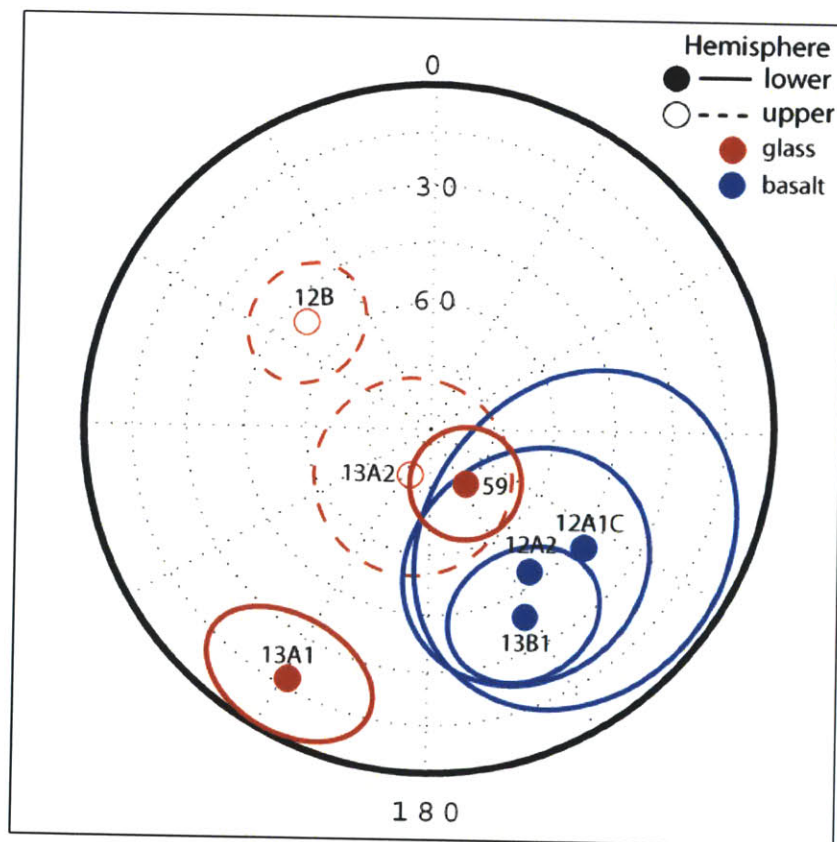Equal-area plot showing directions of LC components. Equal-area plots are stereographic representations.

Figure 15: HC Components

This equal area plot shows the HC components for each sample. The maximum angular deviation (MAD) for each component is also shown.
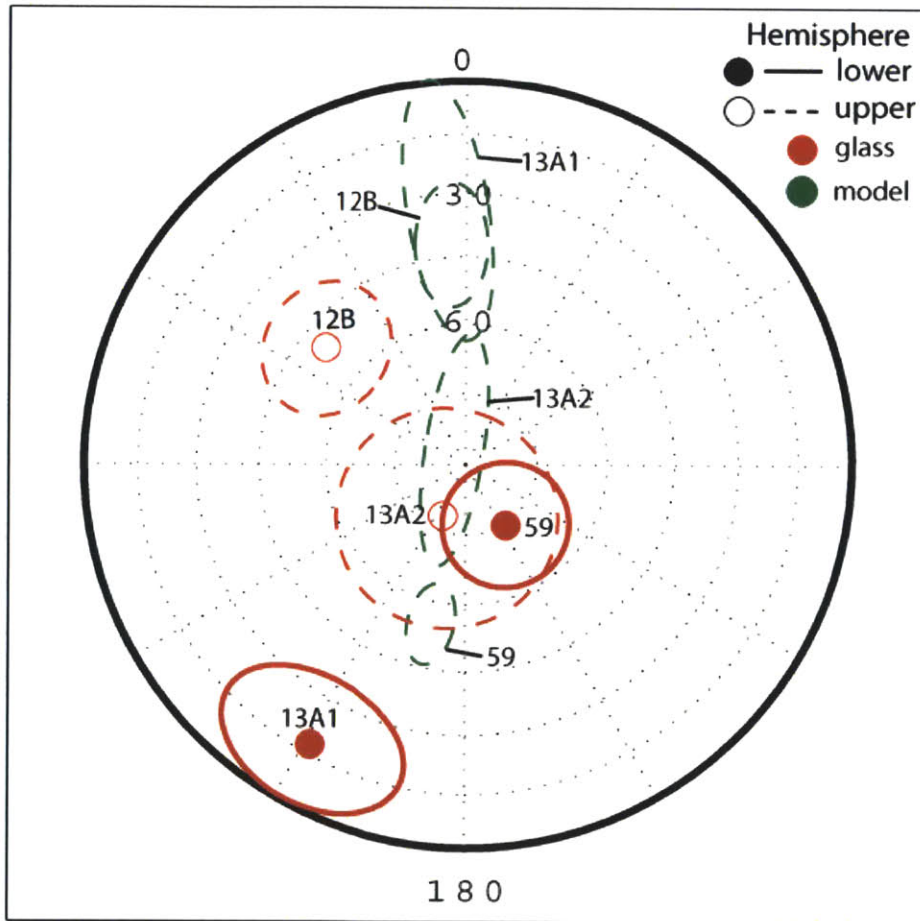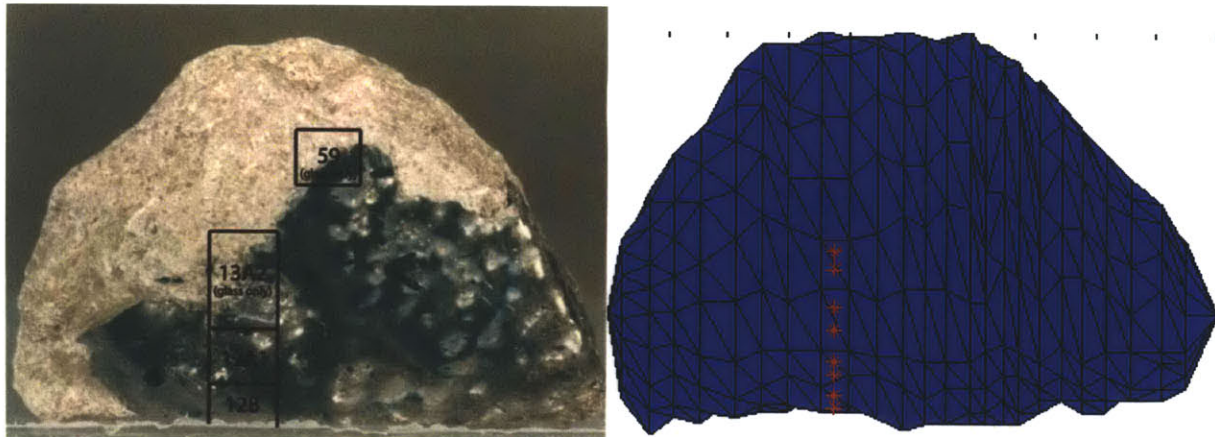
Figure 13: Model Predicted Directions

a) Location of glass samples on whole rock. b) Path of calculations on model. c) Equal area plot showing the model predicted directions (green ellipses) for the various samples and the directions determined by demagnetization. Note the general clustering of the model predicted directions and the scatter of the observed HC directions. Some samples lie close to their model predicted directions (12B and 13A2).

Table 1: Magnetization Components

Sample	Basalt Or Glass	Mass (mg)	Compo-nent	Range (mT)	Forced through origin?	Dec (°)	Inc (°)	n	Max. Ang. Dev.
12A	Basalt	503	Sanding	n/a	No	249	-38.8	6	27.2
12A1C	Basalt	104.3	LC	NRM-8	No	239.9	81	15	11
			HC	8.5-64	Yes	127	43.6	73	39.5
12A2	Basalt	183.0	LC	NRM-8.5	No	249.5	33.7	16	12
			HC	8.5-69	Yes	145.7	48.1	77	29.1
12B	Glass	27.1	Sanding	n/a	No	348.8	66.2	5	24
			LC	NRM-8.5	No	277.8	24.7	16	9.8
			HC	9-58	Yes	346.8	-65.1	75	20.5
13A	Glass	132.9	Sanding	n/a	No	4.8	-7.6	14	27.2
13A1	Glass	69.9	LC	NRM-7	No	302.8	16.8	13	6.1
			HC	7.5-85	Yes	209	17.7	106	17
13A2	Glass	49.5	LC	NRM-8.5	No	269.9	21.1	16	14
			HC	8.5-85	Yes	206.4	-78.6	103	23
13B	Basalt	131.6	Sanding	n/a	No	135.6	36.2	13	23.3
13B1	Basalt	131.6	LC	NRM-11.5	No	263.8	-17.4	21	36.9
			MC	12-54	No	121	-70.7	66	35.4
			HC	54-80	Yes	144.9	26.9	26	22
59	Glass	~15*	LC1	NRM-4.5	No	180	-11.4	7	9.4
			LC2	5-9	No	303.6	-3.9	9	15.8
			HC	9.5-39	Yes	146.5	74.6	56	13.3

*estimated

Table 2: Fisher Statistics

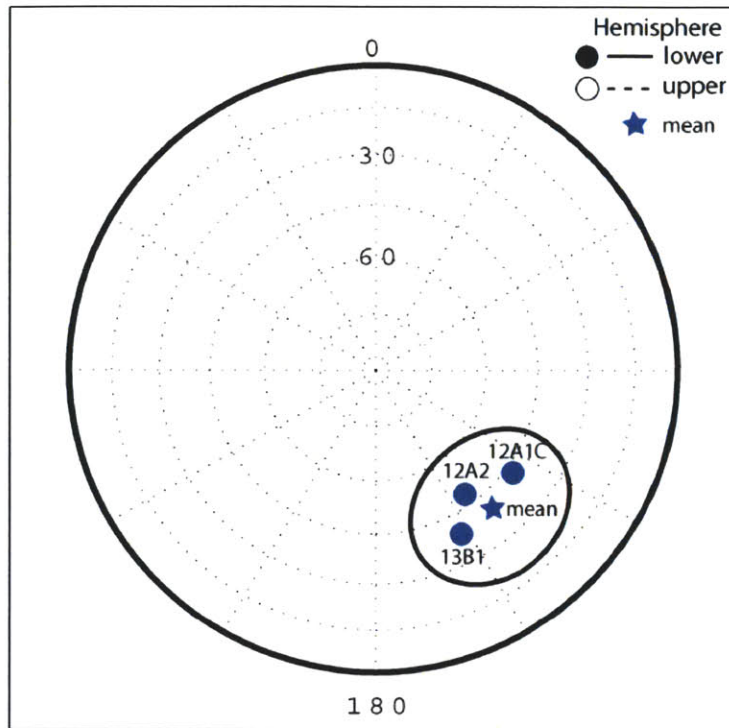|	Components	Dec (°)	Inc (°)	α95 (°)	κ	n
Overprint	LC	284.3	22.3	27.4	4.77	7
Basalt Mean Magnetization	HC	139.4	39.6	21.1	23.44	3

Figure 17: Basalt Mean Direction

Equal area plot showing the basalt HC components and the mean direction of these components. The alpha-95 confidence ellipsoid is also shown.

Paleointensities

We calculated the strength of the magnetizing field for basalt and glass subsamples and for both HC and LC components. The strength of the magnetizing field responsible for the LC component is estimated to be between 0.1 and 0.3 mT, using both ARM and IRM paleointensity methods (assuming it is a TRM), and is consistent in both basalt and glass subsamples. The strong value argues against a TRM origin and is typical of IRM. The agreement in direction and intensity amongst both lithologies further strengthening the idea that the LC component was acquired post emplacement of the glass. The fact that samples separated in 1970 have LC components in a consistent absolute direction indicates the component was acquired before subsampling. Such a secondary IRM overprint has been found on many Apollo subsamples and was likely acquired during transfer from the Moon to the Earth [34]. This strength estimate is only accurate to within an order of magnitude. The strength of the HC fields, however could not be isolated in either basalt or glass samples. Upper limits on the strength of the magnetizing field are 50 µT and 10 µT for the basalt and glass respectively. These upper limits were calculated using the recording properties of the rocks. The rocks cannot accurately record fields below these limits. The calculated paleointensities of the samples were 40 µT and 1 µT for basalt and glass, respectively, which is below the reliable range of strengths (Figure 14, Table 3).

33

NRM lost v ARM gained- Sample 12B (glass)
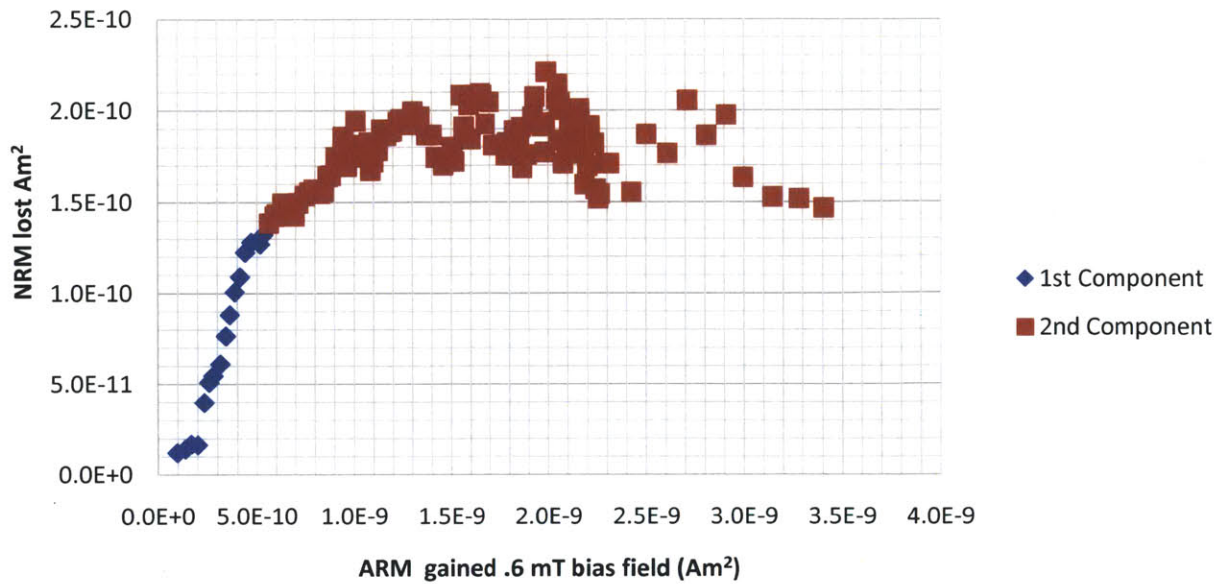
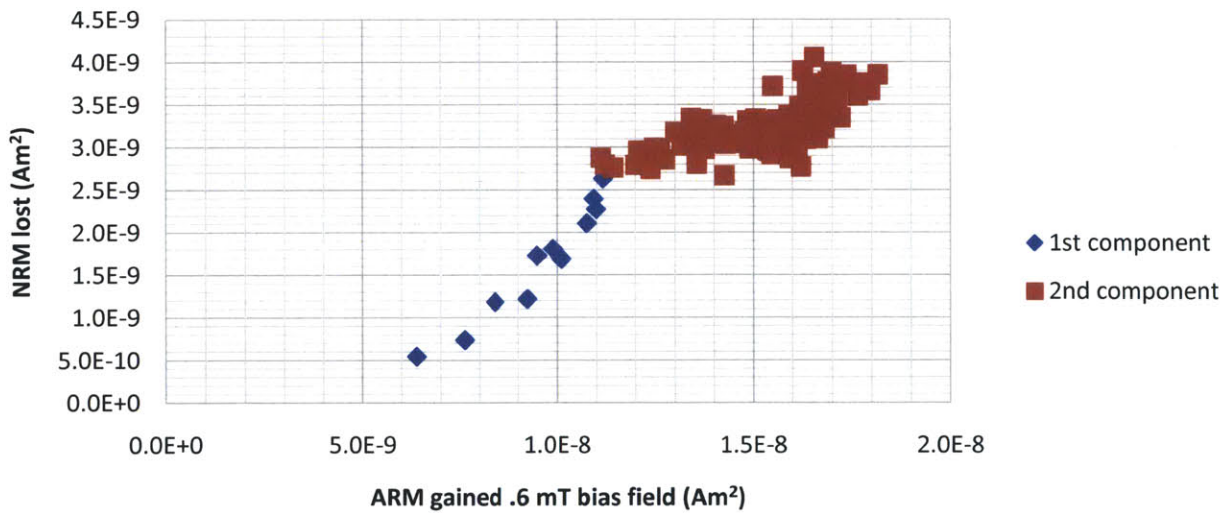**NRM lost v ARM gained- Sample 12A2 (basalt)**

Figure 14: Paleointensity Plots

From the slope of the lines we were able to compute the intensity of the paleofields.

Table 3: Synthetic Paleointensity Experiments

Yellow boxes indicate where the samples could not accurately record the synthetic field.

Glass (Sample 12B):

Paleofield (μT)	12.17	8.22	15.83	31.08	72.98
Synthetic (μT)	2.23	7.46	14.92	37.31	74.62
Percent difference	-443.8	-10.2	-6.1	16.7	2.2

Basalt (Sample 12A2):

Paleofield (μT)	24.7	45.4	45.3	68.4
Synthetic (μT)	7.5	14.9	37.3	74.6
Percent difference	-230.6	-203.9	-21.28	8.34

Glass (Sample 13A2):

Paleofield (μT)	1.37	5.11	3.97	44.94	82.08
Synthetic (μT)	2.23	7.46	14.92	37.31	74.62
Percent difference	0.38	0.314	0.734	-0.20	-0.1

CONCLUSIONS

We were not able to determine the method of magnetization of the 12017 glass. Even with current state-of-the-art AF methods, the fields recorded in this sample, and possibly many other lunar samples, are too weak to be recovered. This results in overestimated paleointensity determinations. It is possible that magnetization acquired by young lunar rocks is from interaction fields from older magnetized rocks nearby or background laboratory fields. Therefore, young lunar samples cannot be used as arguments against an ancient core dynamo. Although the magnetic recording abilities of the 12017 basalt are questionable, the unidirectionality of magnetization between our subsamples and those measured by [32] imply the presence of a long-lived field on the Moon at 3.2 Ga, possibly from a core dynamo.

1.   C. K. Shearer *et al.*, *Reviews in mineralogy and geochemistry* **60**, 365 (2006).
2.   J. A. Wood, in *Origin of the moon*. (Kona, HI, 1986), vol. 1, pp. 17-55.
3.   M. Pritchard, D. Stevenson, *Origin of the Earth and Moon*, 179 (2000).
4.   J. G. Williams, S. G. Turyshev, D. H. Boggs, J. T. Ratcliff, *Advances in Space Research* **37**, 67 (2006).
5.   R. C. Weber, P.-Y. Lin, E. J. Garnero, Q. Williams, P. Lognonné, *Science* **331**, 309 (January 21, 2011, 2011).
6.   C. T. Russell, R. L. McPherron, R. K. Burton, *J. Geophys. Res* **79**, 1105 (1974).
7.   D. A. Crawford, P. H. Schultz, *International journal of impact engineering* **23**, 169 (1999).
8.   S. M. Cisowski, D. W. Collinson, S. K. Runcorn, A. Stephenson, M. Fuller, *Proc. Lunar Planet. Sci. Conf. 13th*, A691 (1983).
9.   I. Garrick-Bethell, B. P. Weiss, D. L. Shuster, J. Buz, *Science* **323**, 356 (2009).
10. M. A. Wieczorek *et al.*, in *Rev. Mineral. Geochem.* (2006), vol. 60, pp. 221-364.
11. C. Dwyer, D. Stevenson, F. Nimmo, in *AGU*. (San Fransisco, Ca, 2010), vol. 1, pp. 02.
12. W. K. Hartmann, Ed., *Moons and planets*, (Wadsworth Publishing Co., ed. 2, 1983), 2, pp. 526.
13. L. Tauxe, *Essentials of paleomagnetism*. (University of California Press, 2010).
14. R. F. Butler, *Paleomagnetism: magnetic domains to geologic terranes*. (Blackwell Scientific Publications, 1992), vol. 319.
15. G. Pearce, D. Strangway, *NASA Special Publication* **315**, 755 (1972).
16. J. Gattacceca *et al.*, *Earth and Planetary Science Letters*, (2010).
17. A. Stephenson, *Journal of Geophysical Research* **98**, 373 (1993).
18. A. Stephenson, D. Collinson, *Earth and Planetary Science Letters* **23**, 220 (1974).
19. Y. Yu, *Geochem. Geophys. Geosyst.* **11**, Q02Z12 (2010).
20. A. Stephenson, S. Runcorn, D. Collinson. (1977), vol. 8, pp. 679-687.
21. J. Warner, *Apollo 12 Lunar Sample Information*. (NASA Curatorial Branch Publication #, Houston, 1970), pp. 391.
22. J. W. Morgan, J. C. Laul, R. Ganapathy, E. Anders, *Science* **172**, 556 (May 7, 1971, 1971).
23. W. Baldridge, D. Beaty, S. Hill, A. Albee, in *Lunar and Planetary Science Conference*. (New York, Pergamon Press, Houston, TX, 1979), vol. 10, pp. 115-139.
24. J. Rhodes, J. Brannon, K. Rodgers, D. Blanchard, M. Dungan, in *Lunar Science Conference*. (New York, Pergamon Press, Houston, TX, 1977), vol. 8, pp. 1305-1338.
25. P. Horn, T. Kirsten, E. Jessberger, *Meteoritics* **10**, 417 (1975).
26. D. A. Morrison, D. S. McKay, R. M. Fruland, H. J. Moore, *Proc. Lunar Sci. Conf. 4th*, 3235 (1973).
27. R. L. Fleischer, H. R. Hart, G. M. Comstock, A. O. Evwaraye, *Proc. Lunar Sci. Conf. 2nd*, 2559 (1971).
28. F. Horz, E. Schneider, D. Gault, J. Hartung, D. Brownlee, *The Moon* **13**, 235 (1975).
29. C. B. Sclar, in *Lunar Science Conference* (Houston, TX, 1971).
30. E. Anders, R. Ganapathy, R. R. Keays, J. C. Laul, J. W. Morgan, in *Lunar Science Conference*. (MIT Press, Houston, TX, 1971), vol. 2, pp. 1021-1036.
31. T. L. Grove, D. Walker, *Proc. Lunar Sci. Conf. 8th*, 1501 (1977).
32. D. Strangway, G. Pearce, W. Gose, R. Timme, *Earth and Planetary Science Letters* **13**, 43 (1971).
33. C. T. Barnett, *Geophysics* **41**, 1353 (1976).
34. G. Pearce, W. Gose, D. Strangway. (1973), vol. 4, pp. 3045.